Broadband Synthetic Aperture Scanning System for Three-Dimensional Through-the-Wall Inspection

Jaime Laviada, Ana Arboleya, Fernando López-Gayarre, and Fernando Las-Heras, *Senior Member, IEEE*

***Abstract*—This letter presents a cost-effective technique for through-the-wall imaging of objects beyond a wall. The approach relies on an amplitude-only multi-monostatic radar that operates as a synthetic aperture radar. In contrast to conventional approaches, the system employs recent broadband techniques for phase retrieval. Thus, the complexity of the scanner is reduced whereas it preserves the capacities of a conventional broadband system to retrieve the three-dimensional profile of objects. Moreover, the system is compatible with state-of-the art techniques that require full (i.e., amplitude and phase) acquisitions. Results at different frequency bands are shown to illustrate how the system can provide accurate estimation of the profile of metallic objects behind building materials such as plywood, plasterboard or hollow bricks and mortar.**

***Index Terms*—Through-the-wall imaging; synthetic aperture radar; monostatic; phase retrieval.**

I. Introduction

THROUGH-the-wall imaging has been mainly employed to detect the presence of people behind walls [1], [2]. In general, it has been achieved by means of electromagnetic waves up to 10GHz [1]. Nevertheless, the recent advances in higher frequency components, mainly at millimeter and submillimeter-wave bands, have enabled higher resolution capabilities at the expense of a shorter range. These new characteristics have opened up new possibilities involving *through-the-wall inspection* to detect hidden and illegal materials such as explosives, contraband or listening devices, which could be hidden behind and close to building materials [3].

In general, imaging based on electromagnetic waves can be accomplished by either using an antenna with a small spot (usually by means of lenses, e.g., [3]) or by using non-directive antennas with a large spot and processing the information by means of *synthetic aperture imaging*. This latter technique is widely used (e.g.,[1], [4], [5], [6]) and its major advantage is the capacity to focus at an arbitrary distance in contrast to the lenses which are usually optimized to focus at a fixed distance.

In through-the-wall inspection, it is advantageous to provide not only lateral resolution, which is given by the working frequency, but also depth resolution to find the distance to the hidden object. Nevertheless, depth resolution is proportional to the bandwidth of the signal [7] and, therefore, it is advisable to resort to a system based on broadband components to achieve the best resolution possible. In general, *power detectors*, which are only able to measure the amplitude of the received signal, enable a wider bandwidth compared to standard I/Q mixers, which are able to measure the amplitude as well as the phase of the received signal. Nevertheless, *synthetic aperture imaging* requires phase information [7].

Although the use of amplitude-only radar is convenient for a three-dimensional wall-inspection, an appropriate *phase retrieval* technique is required. Despite a large collection of techniques is available in the literature (e.g., [8], [9]), the work of approaches compatible with *phaseless and broadband* imaging has been very limited to the best knowledge of the authors. Nonetheless, a novel technique, which can operate with multifrequency monostatic imaging based on amplitude-only data, has been recently proposed [10].

The main *contribution* of this work is the demonstration of the capability of amplitude-only scanners to accurately compute the three-dimensional reconstruction of objects behind a wall. For this purpose, the model proposed in [10] is implemented by a microstrip circuit as well as by off-the-shelf components. In addition, the phase retrieval algorithm is modified so that the system does not require a variable attenuator in contrast to [10].

II. Scanning system

A. Modified quasi-monostatic scanning setup

The *synthetic aperture* approach employed in this paper is detailed in Fig. 1. A transmitter and receiver, which are connected by a reference signal, are moved along a plane parallel to the wall. This plane is referred to as *scanning surface*. A distance d has been intentionally left between the scanning surface and the wall in case reflections could affect the correct operation of the antennas. Otherwise, this safety distance can be reduced to zero.

In this system, the transmitter and receiver antennas are close to each other in a *quasi-monostatic* arrangement. An interferometric signal is obtained by combining the received signal, which is the result of the waves reflected by the wall and the objects behind, with a fraction of the transmitted signal. The latter signal is usually known as *reference signal*. The scheme of the circuit employed to combine both signals, which is based on standard microwave components, as detailed in [10], is shown in the inset of Fig.1. Thus, a directional coupler and a power combiner are the main components that are required.

In addition, a variable attenuator is usually included in the reference signal branch [10]. The goal of this component

This work has been supported by the Ministerio de Ciencia e Innovación of Spain /FEDER under projects TEC2014-55290-JIN; by the Gobierno del Principado de Asturias (PCTI)/FEDER-FSE under project GRUPIN14-114 and Grant BP11-169.

Jaime Laviada, Ana Arboleya and Fernando Las Heras are with the Departamento de Ingeniería Eléctrica, Universidad de Oviedo, Spain. Fernando López-Gayarre is with the Departamento de Construcción e Ingeniería de Fabricación, Universidad de Oviedo, Spain.

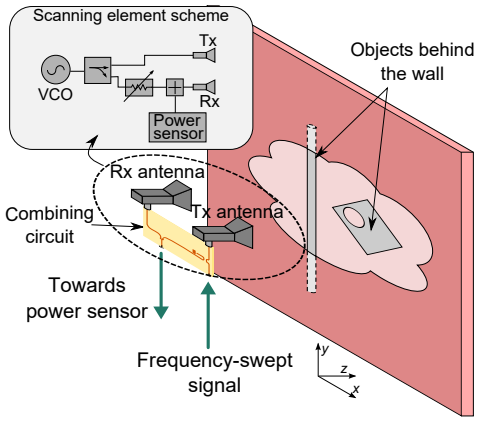

Figure 1. Synthetic aperture radar for through-the-wall imaging.

is twofold. First, it enables to balance the power between the scattered signal and the reference signal. Second, when operating at maximum level of attenuation, it enables to acquire only the intensity of the scattered signal, which is required in the phase retrieval approach originally proposed in [10]. However, in the next section, it will be described how a modified version of the phase retrieval, which does not resort to a variable attenuator, is also effective for the through-the-wall problem under consideration.

B. Phase retrieval

The system described in Fig. 1 enables the acquisition of the power of a signal composed of two components, one corresponding to the monostatic scattered field, which is the signal whose amplitude and phase must be retrieved, and the other one corresponding to the reference signal. Hence, the received power can be assumed to be given by [10]:

$$I\left(\vec{r},\omega\right)=\left|E_S\left(\vec{r},\omega\right)+E_R\left(\omega\right)\right|^2, \tag{1}$$

wherein E_S is the scattered field, E_R is the reference field at the (coupled) output port of the directional coupler, ω is the angular frequency and $\vec{r}$ is the position of the scanning element. In the original phase retrieval approach of [10], the value of the variable attenuator is changed for each position of the scanning element to improve the balance between both branches and, consequently, to improve the dynamic range. Nevertheless, the power of the scattered field in through-the-wall inspection is dominated by the field reflected by the wall and, consequently, it is mainly constant along the scanning surface. Thus, the variable attenuator voltage is set at the beginning of the acquisition and it remains fixed along the acquisition. Although the dynamic range is expected to be lower than in the case of considering the variable attenuator, it will be demonstrated that the system is still able to successfully identify objects behind a wall with good resolution at distances of several tens of centimeters for the considered frequencies (K_u and K_a bands).

Since the value of the reference signal does not change along the measurement, it would be of interest to consider a system without a variable attenuator. In this setup, the balance between the power from both branches would be directly controlled by the coupling coefficient (a fixed value) of the directional coupler.

Nevertheless, this setup entails some challenges because there is no possibility of measuring the amplitude of the scattered field independently from the reference signal in a single scan and, therefore, the algorithm detailed in [10] cannot be applied. To bypass this problem, we will resort to the technique proposed in [11], which takes advantage of the effective time-limited property of the scattered signal. Thus, the modified hologram is computed as:

$$\begin{aligned} I_m\left(\vec{r},\omega\right) &= I\left(\vec{r},\omega\right)-\left|E_R\left(\omega\right)\right|^2 \\ &= E_S\left(\vec{r},\omega\right)\bar{E}_R\left(\vec{r},\omega\right)+\bar{E}_S\left(\vec{r},\omega\right)E_R\left(\vec{r},\omega\right)+ \\ &+ \left|E_S\left(\vec{r},\omega\right)\right|^2, \end{aligned} \tag{2}$$

where the upper bar denotes complex conjugate. The square amplitude of the reference signal $\left|E_R\left(\omega\right)\right|^2$ can be easily characterized when there is not any scatterer nor the wall in front of the scanning element.

If the components of the reference branch have a low dispersive behavior, i.e., the ripple in the amplitude frequency response is moderated and their phase response has a linear dependency on the frequency, then the reference branch contribution can be modeled as:

$$E_R\left(\omega\right)=Ae^{-j\omega t_d}, \tag{3}$$

wherein A is the amplitude of the frequency response and t_d accounts for the delay of the signal to propagate from the VCO to the power sensor. Thus, the inverse Fourier transform of (2) is given by three terms:

$$\begin{aligned} i_m\left(\vec{r},t\right) &= Ae_S\left(\vec{r},t-t_d\right) \\ &+ Ae_S\left(\vec{r},-t+t_d\right)+e_S\left(\vec{r},t\right)*e_S\left(\vec{r},-t\right), \end{aligned} \tag{4}$$

where the operator $*$ denotes convolution. In the previous equation, it has been assumed, without loss of generality, that the complex amplitude A has zero phase.

Fig. 2 depicts these terms, where $\Delta\tau$ is the length of the signal corresponding to the scattered field in the time-domain. In this picture, the same notation as in [10] is used. Thus, the time delay of the reference signal is denoted by t_d and the minimum propagation delay due to the wave traveling from the transmitter to the object and from the object to the receiver, is denoted by t_{min} (see [10] for further details). It is clear that, as long as the central term does not overlap with the other two symmetric terms, the scattered field can be retrieved by means of time gating. This condition can be expressed as $t_d < t_{min}-\Delta\tau$.

In the particular case of through-the-wall inspection with the quasi-monostatic element depicted in Fig. 1, the time delay of the reference signal t_d is expected to be low due to the short distance between the transmitter and receiver antennas and, consequently, the previous condition is met in practice.

If the reference branch has been characterized in a first stage by means of either a network analyzer or a scalar calibration algorithm [12], then, after time gating the modified hologram, it is possible to retrieve the amplitude and phase of the scattered signal by dividing the right term of the signal by the reference signal as detailed in [10].

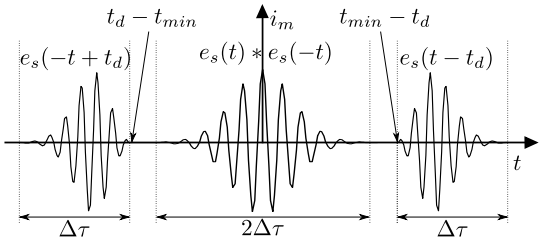

Figure 2. Modified hologram in the time-domain.

C. Interferometry circuit

In order to implement the microwave circuit detailed in Fig. 1, two options are considered. In the case of the K$_\mathrm{a}$-band, a microstrip circuit, consisting of two coupled lines and a Wilkinson divider, is built. The employed substrate is Arlon 25N with a thickness of $203\,\mu$m. The circuit is designed to provide a coupling factor between -40 dB and -50 dB since it has been observed that the reflected signal suffers a similar loss in the considered walls and distances. Two low-directivity horn antennas separated by 5.5 cm have been used. The complete scanning element is shown in Fig. 3.

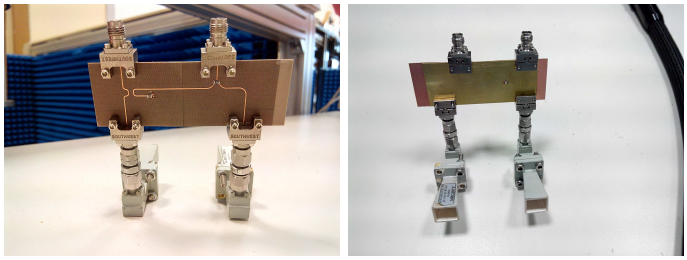

(a) Rear view. (b) Front view.

Figure 3. Implementation of the scanning element at the Ka-band .

In the case of the K$_\mathrm{u}$-band, an alternative solution based on off-the-shelf components has been considered. In this case, the variable attenuator has been included. Two possible values of the variable attenuator have been considered. The first one enables to balance the reference and scattered signal branches. The second one corresponds to the maximum attenuation level so that the scattered signal power can be acquired, enabling the processing described in [10]. The employed components are a directional coupler Agilent 87301D, a power combiner Narda Microwave 4456-2 and two variable attenuators Hittite HMC985LP4KE. Components are connected by means of standard flexible coaxial cables. It is relevant to observe that a long delay line (a 1.5 m coaxial cable) has been introduced between the variable attenuator and the power combiner so that the two components $e_S(t-t_d)$ and $e_S(-t+t_d)$ of the modified hologram are swapped. This choice has been selected because due to the arrangement of the chosen off-the-shelf components a short delay for the reference signal could not be guaranteed and, consequently, it could result in the overlap of the terms in (4). The only effect of this long delay line in the postprocessing is that the time-gating must be applied to the left term of the time-domain modified hologram depicted in Fig. 2 as discussed in [13]. In this implementation, the separation between the antennas is 14.5 cm. A picture illustrating this setup is shown in Fig. 4.

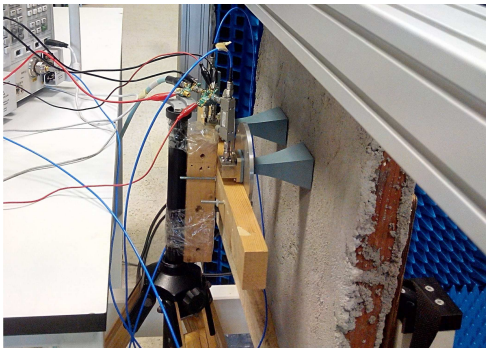

Figure 4. Implemented setup at the Ku-band with off-the-shelf components.

D. Postprocessing

In order to retrieve the amplitude and phase of the scattered field, a *calibration* is firstly required to characterize the reference signal. This calibration can be carried out by either measuring $E_R(\omega)$ with a vector network analyzer (VNA) or by means of the scalar measurement of a reference object under test (OUT) as detailed in [12]. It is important to note that the calibration is required only once.

Once the reference signal has been characterized, the phase can be retrieved *at each spatial point* by means of the next steps:

1) Measure the power of the hologram given by (1).
2) Compute the modified hologram given by (2).
3) Calculate the inverse Fourier transform of the modified hologram to translate the signal to the time domain.
4) Apply a time gating to retain the term $e_s(t) * e_r(-t)$.
5) Compute E_s by calculating the Fourier transform of the term from the previous step and dividing the result by $E_R^*(\omega)$.

After retrieving the phase, the imaging is carried out by using standard synthetic aperture imaging techniques as described in [7]. Since imaging algorithms do not demand *frequency sampling rates* as high as the one considered for the phase retrieval [7], [10], the data can be subsampled in the frequency domain to speed up the creation of the image. It is important to remark that the previous algorithm relies on considering free space and it does not take into account propagation through other mediums. Although it provides good results as shown in the next section, several algorithms can be applied to achieve further improvements by compensating the wall propagation [14], spatial filtering [15] or the possibility to include two different ray propagation constants in the formulation [16]. Differential SAR [5] has also shown good results to remove the approximately constant reflection due to the field scattered by the wall.

Since standard synthetic aperture imaging is used, depth and lateral resolutions are given by well-known formulas [7]. According to this, the radar will be able to detect objects as long as they are behind the wall at a distance larger than the depth resolution $\Delta z = c/2B$ [7], being c the speed of

light and B the bandwidth of the measurement. On the other hand, lateral resolution is mainly a function of wavelength and the raster scan surface [7] and, therefore, imaging capabilities are not expected to be degraded due to moving away some centimeters the objects under test from the wall.

III. Results

In this section, two demonstrators are presented to validate the system previously described. The first demonstrator operates at the K_a band that exhibits good penetration capabilities for 'weak' scattering materials such as plasterboard or wood. However, the high propagation losses make it not recommendable to analyze other kind of walls (see [17] for further details on the constitutive parameters of conventional building materials). In this demonstrator, the previously described microstrip circuit is used as combining circuit.

A second demonstrator is implemented at the K_u band, which exhibits better penetration capabilities. However, since the resolution of the system is proportional to the center wavelength, worse resolution is expected. In this case, the setup is completely implemented by means of off-the-shelf components. Both frequency bands have been sampled with 201 frequency points that have been observed to provide a correct phase retrieval in both cases.

Although a final system would perform raster scanning by moving the antennas along the wall, in these demonstrators, the antennas remain static and the object is moved along a plane. This approach is equivalent to move the antennas while the object remains static if the wall is (effectively) homogenous such as in the case of wood or plasterboard. In the case of non-homogenous materials such as building material containing bricks, it results in a fair approximation.

In both demonstrators, the spatial sampling rate is set at $\Delta x = \Delta y = \lambda_{min}/4$ wherein λ_{min} is the shortest wavelength, i.e., the wavelength at the maximum frequency. The object under test consists, in all the cases of study, on a square plate of 10 cm with a hole of diameter equals to 4 cm together with a cylinder of radius 1.6 cm. Both objects are fastened to a piece of cardboard by means of masking tape as shown in Fig. 5. The input and output of the scanning element are connected to a VNA. Nevertheless, the phase is discarded to emulate the data acquired by a power detector.

For the sake of completeness, the statistical parameters of the background reflectivity, measured in the volume at a minimum distance of 10 cm from the object in the x-axis and 5 cm from the wall are shown in Table I.

Table I
STATISTICAL BACKGROUND REFLECTIVITY.

Material	Mean	Stand. deviation	Max.
Plasterboard	-32.56 dB	5.20 dB	-19.40 dB
Plywood	-26.96 dB	5.71 dB	-15.39 dB
Hollow bricks and mortar	-19.89 dB	7.88 dB	-4.32 dB

A. K_a band results

This first demonstrator is implemented at the K_a band that ranges from 26.5 GHz to 40 GHz (see Fig. 5). The aperture of the antennas is placed at 6 cm from the wall whereas the objects are placed 10 cm behind the wall. The gain of each antenna is 10 dB and the beamwidth is $55°$ for the E and H planes. The scanning surface, i.e., the surface along which the object is moved, is a rectangular plane with dimensions of 16.5 cm and 64 cm for the x and y coordinates, respectively.

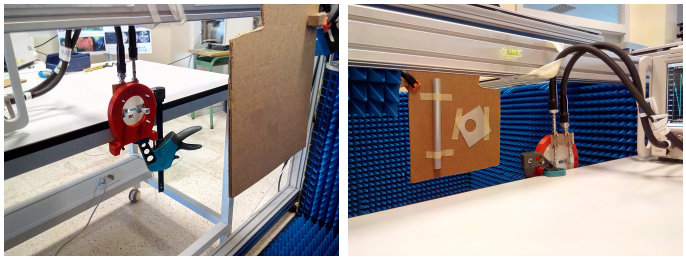

(a) Front view (b) Rear view

Figure 5. Setup implemented at the K_a band without the building walls.

The materials of the walls considered in this demonstrator are plasterboard and plywood. In both cases, the thickness is 1.3 cm. In this frequency range, the measured mean attenuation for each material is 1.17 dB and 7.93 dB, respectively. Fig. 6 shows the setup after including the materials between the antennas and the object.

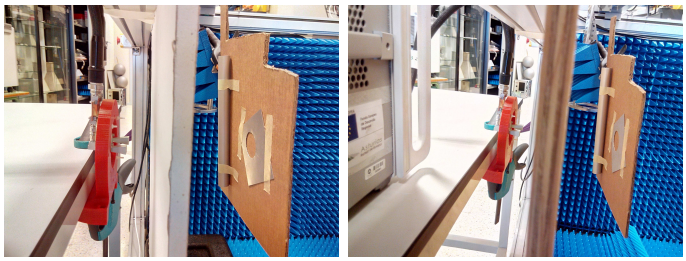

(a) (b)

Figure 6. Setup implemented at the K_a including the walls: a) plasterboard; b) plywood.

After the phase retrieval, the first and last eleven frequencies are discarded since they are expected to be contaminated by some error [10]. Next, the reflectivity is calculated by using only 90 frequencies. The results for both materials are shown in Fig. 7 with a very good agreement with the real OUT.

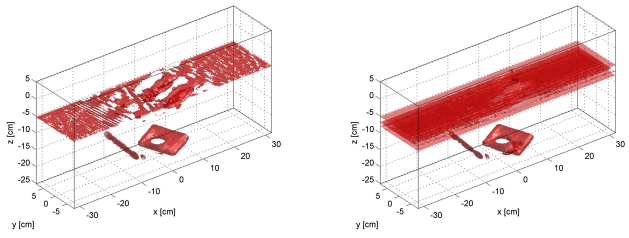

(a) (b)

Figure 7. Computed reflectivity the OUT placed behind a wall of: a) plasterboard; b) plywood. Reconstructed profiles correspond to the isosurface at -8 dB.

B. K_u band results

In this demonstrator, the setup has been implemented at the K_u band to analyze materials exhibiting poor penetration. In

particular, a hollow bricks and mortar wall is considered. The bricks contain a single air chamber and their thickness is 4 cm. The total thickness of the wall, including the concrete layers, is 7 cm. The measured mean attenuation of the wall is 16.46 dB in the $\mathrm{K_u}$ band. Antennas are placed so that the aperture of the horns is on the wall surface and the separation between both antennas is 14.5 cm. The typical gain and beamwidth of each antenna are 16.5 dB and $28.5°$ for the E and H planes. The object under test is placed at 18.5 cm behind the wall.

In this case, the variable attenuators have been introduced and, therefore, it is possible to resort to the original postprocessing scheme detailed in [10] as previously discussed. Fig. 4 shows the implemented setup at this working band.

In this example, the scanning dimensions are 21.84 cm and 59.64 cm for the x and y directions. The frequency band ranges from 12.4 GHz to 18 GHz. After the phase retrieval, the first and last five frequencies are discarded and the resulting field is subsampled again by a factor of two in frequency. Hence, the number of frequencies for the profile reconstruction is 96.

Fig. 8 depicts the computed reflectivity. Despite resolution is poorer than at the $\mathrm{K_a}$ band due to the lower available power and shorter wavelength, the square plate and the cylinder bar can still be clearly identified.

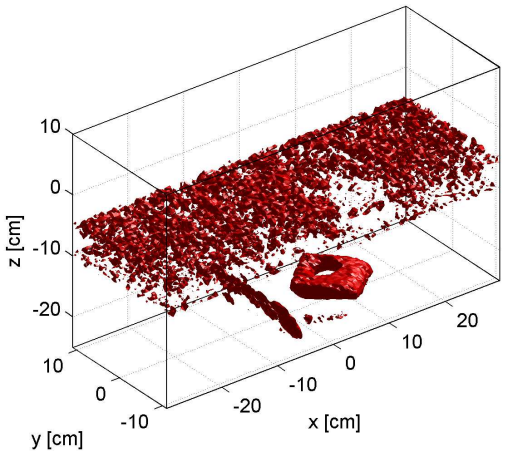

Figure 8. Reflectivity at -6 dB for the bricks and mortar wall.

IV. Conclusions

A simple scheme for non-destructive inspection of objects behind a building wall has been presented in this paper. The approach avoids the use of I/Q mixers and it only relies on power detection. On the one hand, the phase retrieval and profile computation algorithms are based on efficient Fourier transforms and, therefore, they involve a low computational burden. On the other hand, the system can be physically implemented by means of either simple microwave circuitry, which can be manufactured with widespread milling machines, or off-the-shelf components.

The approach has been validated at the $\mathrm{K_u}$ and $\mathrm{K_a}$ bands employing *ad-hoc* microwave circuitry as well as commercial components. The performance of the system reveals a good capability to detect the shape of metallic objects (as pipes) close to walls of conventional materials such as plywood, plasterboard or hollow bricks and mortar. Thus, the system is expected to be compatible with advance postprocessing to compensate the propagation through the walls that could be required in other environments such as the analysis of embedded or buried objects.

Although dielectric objects (e.g., PVC pipes) have not been considered in this work, the setup would remain unchanged. Nevertheless, special care must be paid in the postprocessing since internal reflections and weak reflectivity could result in artifacts degrading the quality of the image.

Acknowledgment

The authors would like to thank Dr. Carlos Vazquez-Antuña, Mr. George Hotopan and Mr. Cebrián García-González for their help in fabricating the microstrip circuit and setting up the components and construction walls.

References

[1] N. Maaref et al., "A study of UWB FM-CW radar for the detection of human beings in motion inside a building," *IEEE Trans. Geosci. Remote Sens.*, vol. 47, no. 5, pp. 1297–1300, May 2009.

[2] F. Adib and D. Katabi, "See through wall with Wi-fi!" in *ACM SIGCOMM'13*, Hong Kong, China, August 12-16 2013, pp. 75–86.

[3] C. Adams, D. Holbrook, and R. Sengsten, "A handheld active millimeter wave camera," in *IEEE International Conference on Technologies for Homeland Security (HST)*, Nov 2010, pp. 283–286.

[4] M. Dehmollaian and K. Sarabandi, "Refocusing through building walls using synthetic aperture radar," *IEEE Trans. Geosci. Remote Sens.*, vol. 46, no. 6, pp. 1589–1599, Jun. 2008.

[5] M. M. Dehmollaian, M. Thiel, and K. Sarabandi, "Through-the-wall imaging using differential SAR," *IEEE Trans. Geosci. Remote Sens.*, vol. 47, no. 5, pp. 1289–1296, May 2009.

[6] T. S. Ralston, G. L. Charvat, and J. E. Peabody, "Real-time through-wall imaging using an ultrawideband multiple-input multiple-output (MIMO) phased array radar system," in *IEEE International Symposium on Phased Array Systems and Technology (ARRAY)*, Oct 2010, pp. 551–558.

[7] J. M. Lopez-Sanchez and J. Fortuny-Guasch, "3-D radar imaging using range migration techniques," *IEEE Trans. Antennas Propagat.*, vol. 48, no. 5, pp. 728–737, May 2000.

[8] L. Crocco, M. D'Urso, and T. Isernia, "Inverse scattering from phaseless measurements of the total field on a closed curve," *J. Opt. Soc. America*, vol. 21, no. 4, pp. 622–631, Apr. 2004.

[9] G. Hislop, L. Li, and A. Hellicar, "Phase retrieval for millimeter- and submillimeter-wave imaging," *IEEE Trans. Antennas Propagat.*, vol. 57, no. 1, pp. 286–289, Jan. 2009.

[10] J. Laviada et al., "Phaseless synthetic aperture radar with efficient sampling for broadband near-field imaging: Theory and validation," *IEEE Trans. Antennas Propagat.*, vol. 63, no. 2, pp. 573–584, 2015.

[11] ——, "Phase retrieval technique for submillimetre-wave frequency scanning-based radar system," *IET Microwave, Antennas, Propag.*, vol. 8, no. 14, pp. 1170–1178, Nov. 2014.

[12] J. Laviada and F. Las-Heras, "Scalar calibration for broadband synthetic aperture radar operating with amplitude-only data," *IEEE Antennas Wireless Propag. Lett*, no. 14, pp. 1714–1717, 2015.

[13] J. Laviada et al., "A novel phaseless frequency scanning based on indirect holography," *J. Electromagn. Waves Appl.*, vol. 27, no. 4, pp. 275–296, 2013.

[14] F. Fioranelli, S. Salous, and X. Raimundo, "Frequency-modulated interrupted continuous wave as wall removal technique in through-the-wall imaging," *IEEE Trans. Geosci. Remote Sens.*, vol. 52, no. 10, pp. 6272–6283, Oct 2014.

[15] Y.-S. Yoon and M. G. Amin, "Spatial filtering for wall-clutter mitigation in through-the-wall radar imaging," *IEEE Trans. Geosci. Remote Sens.*, vol. 47, no. 9, pp. 3192–3208, Sept 2009.

[16] S. C. Henry et al., "Three-dimensional broadband terahertz synthetic aperture imaging," *Optical Engineering*, vol. 51, no. 9, pp. 091 603–1–091 603–9, 2012.

[17] I. Cuiñas and M. G. Sanchez, "Measuring, modeling, and characterizing of indoor radio channel at 5.8 ghz," *IEEE Trans. Veh. Technol.*, vol. 50, no. 2, pp. 526–535, Mar. 2001.